OE Optical Engineering

RESEARCH PAPER

Asymmetric simplified coherent receiver based on twin-single-sideband signal realizes ultra-low computational complexity

Keji Zhou,[a,b,*] **Tianming Li**,[c] **Yaqin Wang**,[c] **Sheng Cui**,[d] **Ming Wei**,[b] **and Yong Xiao**[a]

[a]Huazhong University of Science and Technology, School of Electronic Information and Communications, Wuhan, China

[b]Wuhan Fiberhome Technical Services Co., Ltd., Wuhan, China

[c]Fiberhome Telecommunication Technologies Co., Ltd., Advanced Research Department, Wuhan, China

[d]Huazhong University of Science and Technology, School of Optical and Electronic Information, Wuhan, China

ABSTRACT. Simplified coherence technology based on direct detection has been a hot topic because of its simple structure and low cost. However, some recently proposed simplified coherent receivers (SCRs) require extremely complex mathematical operations, resulting in high power consumption of digital signal processing. We design an asymmetric SCR (ASCR) based on a twin-single-sideband signal, and the field reconstruction algorithm only requires one Hilbert operation, avoiding the nonlinear mathematical operation and the digital up-sampling. Compared to the asymmetric direct detection receiver, the power consumption of the ASCR in the part of optical field reconstruction and dispersion compensation can be reduced by 79.83% under the same sensitivity. Besides, an optimal design of the optical filter and the channel equalization for the ASCR is proposed.

Keywords: simplified coherent receiver; power consumption; field reconstruction algorithm; dispersion compensation; twin-single-sideband

Paper 20230252G received Mar. 17, 2023; revised Sep. 2, 2023; accepted Oct. 13, 2023; published Oct. 31, 2023.

1 Introduction

The demand for ultra-high speed and super-large capacity data transmission is increasing exponentially in optical fiber communication networks. The traditional communication system based on intensity modulation and direct detection has the advantages of a simple system structure and low cost. However, because of its relatively small tolerance for fiber dispersion and other nonlinear effects,[1,2] it is only suitable for short-distance optical transmission scenarios. Optical communication system based on coherent detection and advanced modulation format signal not only has the advantages of high spectral efficiency and high sensitivity[3–8] but also can extensively compensate linear and nonlinear effects in the signal transmission process with digital signal processing (DSP) technology. The current digital coherent optical receiver (DCR) requires two 90 deg optical hybrids, four pairs of balanced photodetectors (BPD), and four analog-to-digital converters (ADCs), resulting in a complex system structure and high cost, which is more suitable for backhaul optical transmission scenarios. It is challenging for a BPD to maintain a high single-port rejection ratio when the symbol rate is higher than 100 Gbaud. Single-ended coherent receiver[9] uses photodectectors (PDs) and digital self-signal beat interference (SSBI) cancellation

*Address all correspondence to Keji Zhou, zhoukj@fiberhome.com

techniques instead of using BPDs. However, the single-ended coherent receiver can not eliminate 90 deg optical hybrids, the system of which is still complex and high cost.

Kramers–Kronig (KK) receiver[10] has attracted much attention as a simplified coherent receiver (SCR) based on direct detection that supports advanced modulation format and high sensitivity.[10–17] KK receiver can reconstruct the entire complex signal field through the relationship between intensity and phase of a minimum-phase signal, therefore, the SCR only needs one PD and one ADC. Compared to the DCR, the KK receiver requires an additional signal field reconstruction algorithm (FRA), which requires digital upsampling and nonlinear mathematical operations. However, the high computational complexity induced by KK-FRA makes real-time DSP too difficult to be applied. Although a few modified KK-FRA[14] without upsampling has been proposed in recent years, it still requires several Hilbert transform (HT) operations in the FRA process, and the computational complexity is still high.

Besides, the KK receiver only suits to single-sideband (SSB) signals, which meet the minimum-phase condition, so the electrical spectral efficiency of the receiver is almost half of the DCR. To overcome the low electrical spectrum efficiency, a symmetric direct detection (SDD) receiver based on left-sideband (LSB) and right-sideband (RSB) signals and KK-FRA is proposed.[18] In this scheme, the optical signal is divided into two lanes, and two independent optical bandpass filters (OBPF) and KK-FRA are used to extract, receive and recover the left and right band signals, respectively. In this system, OBPF with a sharp edge is essential to reduce the cross-talk effect between channels. To reduce the requirement of high-performance OBPF, the multiple-input and multiple-output adaptive equalization (MIMO-AEQ) algorithm is proposed to eliminate the cross-talk,[19] and the paper also points out that the system performance is better when the number of digital filter taps in the MIMO-AEQ reaches 25. Recently, an asymmetric direct detection (ADD) receiver for receiving twin-SSB (TSSB) signals is proposed,[20–23] which requires only one OBPF. The advantage of this approach is that one OBPF is eliminated and the system cost is reduced. However, the signal of LSB requires KK-FRA, while the signal of RSB requires multiple iterations and HT operations, therefore, the computational complexity is much higher than that of the SDD receiver (Fig. 1).

In our previous work, the new FRA used by an SCR achieves ultra-low computational complexity.[24,25] In this paper, based on previous work, we further design an asymmetric SCR (ASCR) based on TSSB signals, it uses a strong local oscillator (LO) to meet pseudo-SSB (PSSB) conditions[24] and eliminate the self-beat and cross-talk noises from LSB and RSB. The FRA of each PSSB signal only requires one HT operation, avoiding the nonlinear mathematical operation and the digital up-sampling required by the KK-FRA. Meanwhile, ASCR eliminates iteration operations required by ADD receiver, and the FRA in the ASCR can be combined with the dispersion compensation algorithm, by which the computational complexity of FRA can be eliminated. Compared to the ADD receiver, the power consumption of the proposed ASCR in the part of optical field reconstruction and dispersion compensation can be reduced by 79.83% under the same sensitivity. In addition, the sensitivity of the two receivers is also compared through simulation and experiment, and the results show that the performance of ASCR is the same as that of ADD receiver. To improve the applicability of ASCR, we also

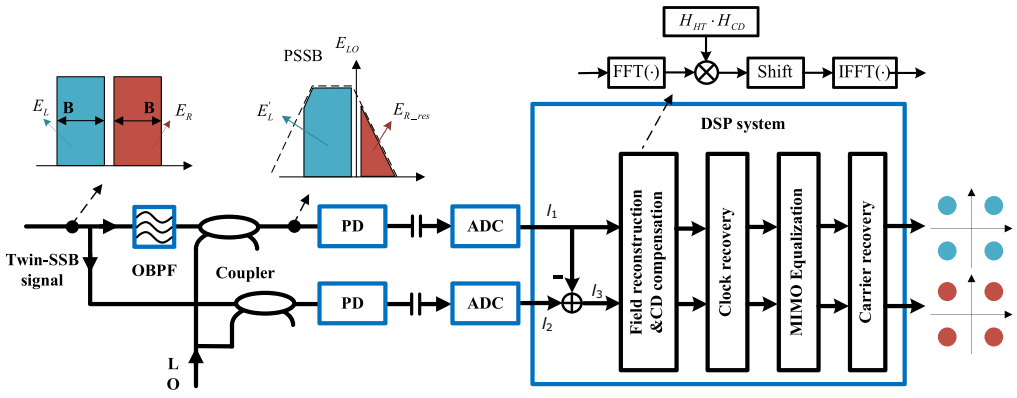

Fig. 1 Structure of receiving TSSB signal (one polarization) within the ASCR.

optimize the number of MIMO taps and the roll-off coefficient of OBPF. The simulation results show that the sensitivity of ASCR is close to the optimal sensitivity when the roll-off factor of OBPF is 200 dB/nm, and the number of MIMO taps is 10.

2 FRA of the ASCR

In the ASCR, the TSSB signal including LSB and RSB, as well as the LO signal field can be expressed as

$$E_{L,R,\mathrm{LO}} = A_{L,R,\mathrm{LO}} \exp j(\omega_{L,R,\mathrm{LO}} t + \varphi_{L,R,\mathrm{LO}}), \tag{1}$$

where $A_{L,R,\mathrm{LO}}$, $\omega_{L,R,\mathrm{LO}}$, and $\varphi_{L,R,\mathrm{LO}}$ are the amplitude, angular frequency, and phase of the signal field, respectively. The TSSB signal in the receiver is first divided into two ways. It is assumed that an OPBF deals with the LSB way, while the other way is without the optical filter. The sampling value of the photocurrent can be expressed as Eqs. (2) and (3) under the condition that the influence of second-order terms is ignored by high LO power

$$\begin{aligned} I_1(n) &= |E'_L(n) + E_{R\_\mathrm{res}}(n) + E_{\mathrm{LO}}|^2 - |E_{\mathrm{LO}}|^2 \\ &= \mathrm{Re}(E'^{*}_L(n)E_{\mathrm{LO}}) + \underbrace{\mathrm{Re}(E_{R\_\mathrm{res}}(n)E^{*}_{\mathrm{LO}})}_{\text{Crosstalk}} + \underbrace{|E'_L(n)|^2}_{\text{SSBI}} + \underbrace{\mathrm{Re}(E'^{*}_L(n)E_{R\_\mathrm{res}}(n))}_{\text{LRBI}}, \end{aligned} \tag{2}$$

$$\begin{aligned} I_2(n) &= |E_L(n) + E_R(n) + E_{\mathrm{LO}}|^2 - |E_{\mathrm{LO}}|^2 \\ &= \mathrm{Re}(E_R(n)E^{*}_{\mathrm{LO}}) + \mathrm{Re}(E^{*}_L(n)E_{\mathrm{LO}}) + |E_L(n)|^2 + |E_R(n)|^2 + \mathrm{Re}(E^{*}_L(n)E_R(n)), \end{aligned} \tag{3}$$

where $E'_L(n)$ and $E_{R\_\mathrm{res}}(n)$ respectively represent the LSB signal and the residual RSB signal after optical filtering, and * represents complex conjugates. Assuming the OPBF is matched with the LSB signal, so $E_L(n) \approx E'_L(n)$. Then the difference value between the two currents can be expressed as

$$\begin{aligned} I_3(n) = I_2(n) - I_1(n) &= \mathrm{Re}(E_R(n)E^{*}_{\mathrm{LO}}) - \underbrace{\mathrm{Re}(E_{R\_\mathrm{res}}(n)E^{*}_{LO})}_{\text{Crosstalk}} + \underbrace{|E_R(n)|^2}_{\text{SSBI}} + \underbrace{\mathrm{Re}(E^{*}_L(n)E_R(n))}_{\text{LRBI}} \\ &\quad - \underbrace{\mathrm{Re}(E'^{*}_L(n)E_{R\_\mathrm{res}}(n))}_{\text{LRBI}}. \end{aligned} \tag{4}$$

$I_1(n)$ and $I_3(n)$ are composed of three parts: linear term, crosstalk term, and nonlinear term. Nonlinear terms include SSBI and left-right sideband beat interference (LRBI). As LO is in the receiver, increasing the LO power is an applicable method to eliminate the influence of SSBI and LRBI. Therefore, under the condition of a high carrier-to-signal power ratio, $I_1(n)$ and $I_3(n)$ can be approximately expressed as

$$I_1(n) \approx \underbrace{\mathrm{Re}(E'^{*}_L(n)E_{\mathrm{LO}})}_{\text{Linear}} + \underbrace{\mathrm{Re}(E_{R\_\mathrm{res}}(n)E^{*}_{\mathrm{LO}})}_{\text{Crosstalk}}, \tag{5}$$

$$I_3(n) \approx \underbrace{\mathrm{Re}(E_R(n)E^{*}_{\mathrm{LO}})}_{\text{Linear}} - \underbrace{\mathrm{Re}(E_{R\_\mathrm{res}}(n)E^{*}_{\mathrm{LO}})}_{\text{Crosstalk}}, \tag{6}$$

where B is the baudrate of LSB and RSB signal, and when $\omega_{\mathrm{LO}} - \omega_L \geq B/2$ and $\omega_R - \omega_{\mathrm{LO}} \geq B/2$ are simultaneously satisfied, the components of $I_1(n)$ and $I_3(n)$ are the real part of PSSB signals. Therefore, according to the PSSB signal optical FRA,[24] the retrieving LSB signal $E_{L\text{-PSSB}}$ and RSB signal $E_{R\text{-PSSB}}$ after fast Fourier transform (FFT), inverse FFT (IFFT), and HT can be expressed as

$$H_{\mathrm{HT}}(k) = \begin{cases} 1, & k = 1, M_H/2 + 1 \\ 0, & k = 2,3,\ldots,M_H/2 \\ 2, & k = M_H/2 + 2,\ldots,M_H \end{cases}, \tag{7}$$

$$E_{L\text{-PSSB}} = \mathrm{IFFT}\{\mathrm{FFT}(I_1(n)) \cdot H_{\mathrm{HT}}(k)\} = E'^{*}_L + E_{R\_\mathrm{res}}, \tag{8}$$

$$E_{R\text{-PSSB}} = \mathrm{IFFT}\{\mathrm{FFT}(I_3(n)) \cdot H_{\mathrm{HT}}(k)\} = E_R - E_{R\_\mathrm{res}}. \tag{9}$$

Therefore, the recovered baseband signals contain inter-symbol interference damage caused by OBPF and crosstalk from RSB, which are shown in Fig. 2(a). These distortions can be

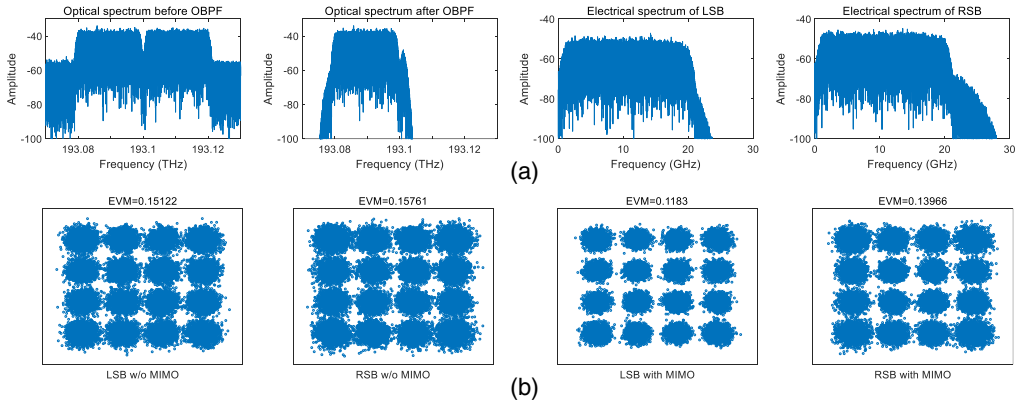

Fig. 2 Optical and electrical spectrum (a) in signal reception. Example error vector magnitude (EVM) of 16 QAM from with or without MIMO (b).

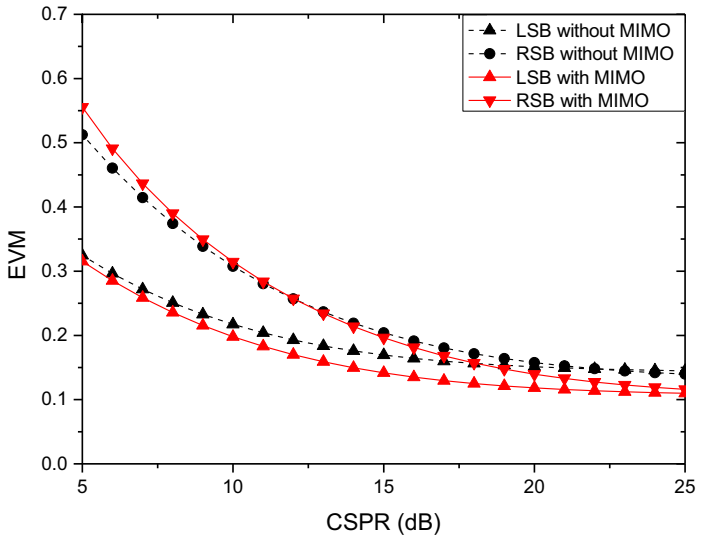

Fig. 3 EVM of LSB and RSB versus CSPR under simulation setup from 16 QAM (OSNR = 30 dB).

eliminated by MIMO-AEQ, which are shown in Fig. 2(b), and it is worth noting that conjugate recovery of E_L must be taken after equalization rather than before, or it will affect the performance of the MIMO-AEQ to eliminate crosstalk.

On the other hand, the second-order term can be ignored in the equation derivation relying on large LO power. As shown in Fig. 3, the optimal receiving performance is achieved when the carrier-to-signal ratio (CSPR) condition is close to 20 dB. Therefore, ASCR is more suitable for the application scenario where the LO is on the receiving side, where the CSPR can easily reach more than 15 dB.

3 Computational Complexity and Power Analysis of the ASCR

ASCR achieves optical field reconstruction by multiplying $H_{\mathrm{HT}}(k)$ in the frequency domain, the specific operation is the same as the frequency domain chromatic dispersion compensation algorithm, so the additional computational load introduced by optical field reconstruction can be eliminated through the fusion with the upper two frequency domain algorithms.[25] Since the demodulation algorithms of the ASCR and the ADD receiver only have differences between the FRA and dispersion compensation algorithm, the computational complexity and power consumption of the two receivers can be directly compared through FRA and dispersion compensation resources.

Assuming FFT and IFFT of radix-4 are used in FRA, the times per point of real number multiplication M and addition A required by FFT and IFFT of N points can be calculated as follows:[26]

$$M[\mathrm{FFT}_{\text{radix-4}}] = \frac{9N\log_2 N}{8} - \frac{43N}{12} + \frac{16}{3}, \tag{10}$$

$$A[\mathrm{FFT}_{\text{radix-4}}] = \frac{25N\log_2 N}{8} - \frac{43N}{12} + \frac{16}{3}. \tag{11}$$

Reconstruction of each sideband requires one FFT and one IFFT. Since the input of FFT is the sampling value of photocurrent, which is a real number signal, its computational complexity can be reduced by half.[27] The computation is negligible for HT when multiplied by the frequency domain $H_{\mathrm{HT}}(k)$, as the transfer function only has 0, 1, and 2. The computation of dispersion compensation can be calculated as a complex multiplication that requires at least three real multiplications and five real additions. Since half of the HT function value is 0, the computation can be reduced by half when multiplied by the whole function.[28] In the final, the average times of real number multiplication and real number addition per point for the ASCR optical field reconstruction and dispersion compensation modules are shown below

$$M[\mathrm{ASCR}] = \frac{1.5 \times M[\mathrm{FFT}_{\text{radix-4}}] + 3 \times M_H}{M_H - 2M_d} = \frac{27M_H\log_2 M_H - 62M_H + 128}{16M_H - 32M_d}, \tag{12}$$

$$A[\mathrm{ASCR}] = \frac{1.5 \times A[\mathrm{FFT}_{\text{radix}-4}] + 5 \times M_H}{M_H - 2M_d} = \frac{75M_H\log_2 M_H - 46M_H + 128}{16M_H - 32M_d}, \tag{13}$$

where M_H represents the block size and M_d represents the number of points that need to be dropped due to the edge effect during block operation.[24] The KK-FRA adopted by the ADD receiver is conducted by the time-domain method,[29] and the same dispersion compensation algorithm to the ASCR is adopted. Therefore, the average times of real number multiplication, real number addition, look-up table per point for the ADD receiver optical field reconstruction, and dispersion compensation modules are shown in Table 1. Where N_S and N_H represent the number of taps of interpolating filter and HT filter, T represents the number of iteration operations, and R represents the up-sampling times.

The same operation consumes different energy due to the different process precision of complementary metal-oxide-semiconductor (CMOS) transistor, so we choose a representative 15 nm CMOS process for power estimation. Under the process precision of 15 nm, the energy consumed by each real number multiplication, real number addition, and look-up table is 0.637, 0.212, and 0.451 pJ, respectively.[29–31] According to the computation statistics in Table 1 and Eqs. (12) and (13), the DSP power estimation curves within different baudrates in Fig. 4 can be obtained. Table 2 lists the specific parameter values for power consumption estimation.

It can be seen that the total power consumption of the ASCR in optical field reconstruction and dispersion compensation is reduced by as much as 79.83% compared with the ADD receiver. Even at 50 Gbaud, the power consumption of ASCR is still only 4.69 W, which leaves enough redundancy for other demodulation modules, which also indicates that the ASCR can well support transmission systems with high baudrate. Meanwhile, the power consumption of the ADD receiver reaches 4.65 W at a 10 Gbaud, and with the increase of baudrate, the power consumption also increases rapidly. Within current DSP technology, it is difficult for a single chip to support the ADD receiver to operate in a transmission system with a high baudrate.

Table 1 Computations in the ADD receiver.

	Field reconstruction	Dispersion compensation
M[ADD]	$\frac{3N_SR}{2} + \frac{N_H(R+T+1)}{4} + 3T + R + 1$	$\frac{27M_H\log_2 M_H - 50M_H + 128}{12M_H - 24M_d}$
A[ADD]	$\frac{3N_SR}{2} + \frac{N_H(R+T+1)}{4} + 2T + R + 1$	$\frac{75M_H\log_2 M_H - 26M_H + 128}{12M_H - 24M_d}$
L[ADD]	$2R$	0

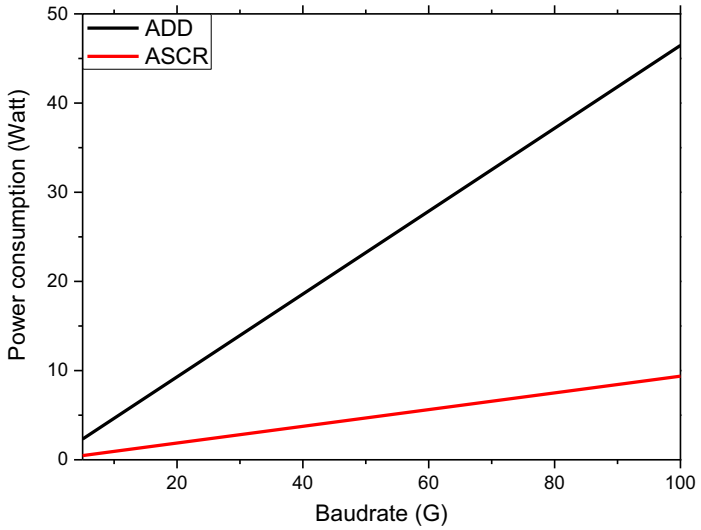

Fig. 4 Power consumption in filed reconstruction and dispersion compensation of the ADD receiver and the ASCR under different baudrates.

Table 2 Parameter values of the ADD receiver and the ASCR in power consumption comparison.

Parameter	M_H	M_d	N_S	N_H	T	R
Value	256	32	11	33	4	2

4 Receiving Sensitivity of the ASCR

According to Fig. 5, the laser of which the central wavelength is 1550.27 nm is used as a carrier and LO simultaneously, and the relative intensity noise is −140 dBc/Hz. The original 10 Gbaud-quadrature phase shift keying (QPSK) LSB and RSB signals are first shaped by Nyquist filtering with a roll-off coefficient of 0.1, and then the frequency shift of 7.5 GHz to the positive or the negative is processed, respectively. Finally, the LSB and RSB signals add in the time domain that the TSSB signal is generated with a 5 GHz guard band. The arbitrary waveform generator with a sampling rate of 40 GSa/s and an analog bandwidth of 25 GHz is used to drive an in-phase and quadrature (IQ) modulator to produce the optical TSSB signal. It is worth noting that, to eliminate the influence of chromatic dispersion and explore the extreme sensitivity performance of the ASCR and the ADD receiver, the experiment was conducted under back-to-back conditions with an LO at the receiving side.

In the receiver part, the TSSB signal is amplified by an erbium-doped optical fiber amplifier of which the noise figure is 6 dB. Then the low-cost OBPF with a bandwidth of 100 GHz and roll-off coefficient of 100 dB/nm is used to filter the majority of amplified spontaneous emission (ASE) noise. After that, the TSSB signal is coupled into two fibers, one lane is without filtering

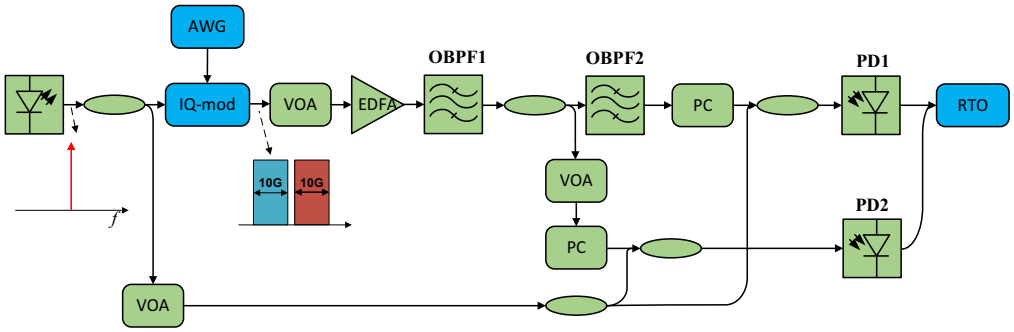

Fig. 5 Sensitivity experiments system diagram for the ASCR and ADD receiver.

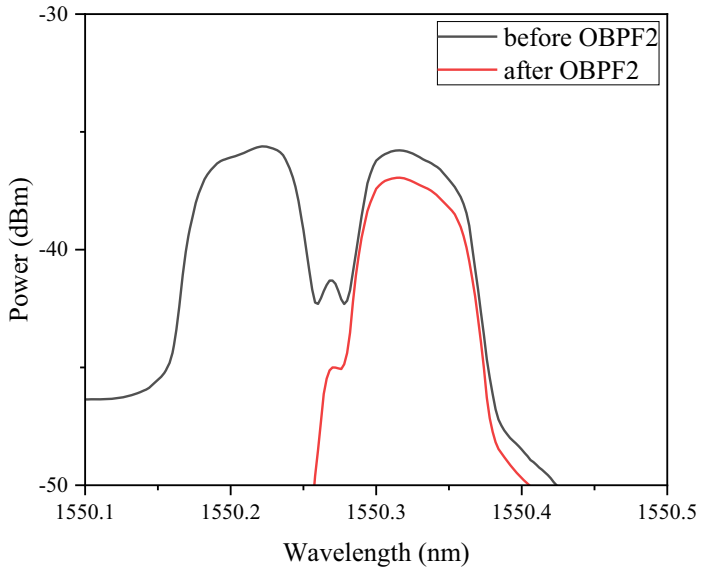

Fig. 6 Optical spectrum of the signals before and after filtering.

and the other lane is with a tunable OBPF to extract the LSB signal. The optical spectrum of the signals before and after filtering is shown in Fig. 6. OBPF2 is XTM-50 from Yenista Optics, and the roll-off coefficient is 500 dB/nm. The two optical signals are polarization controlled and coupled with the LO and finally detected by two PDs, respectively. To eliminate the influence of SSBI and LRBI, a strong LO is used to set the CSPR to 15 dB. A real-time oscilloscope with an 80 GSa/s sampling rate and an analog bandwidth of 36 GHz is used for offline processing.

The experimental results are shown in Fig. 7. It is worth noting that the cross-correlation algorithm is used to align the skew of the two lanes before applying the FRA of the ASCR and the ADD receiver. When the guard band is 4 GHz, which is sufficient to eliminate filtering distortion, the sensitivity of the LSB reaches 8.1 dB for both the ASCR and ADD receiver in the experiments. Due to the filtering bandwidth (<15 GHz) of the tunable OPBF2, the ASE noise of LSB is less compared to that of RSB (>35 GHz), resulting in 0.4 dB sensitivity degradation for both receivers. Simulation results of the ASCR also show the 1.1 dB sensitivity degradation induced by ASE noise. Furthermore, the ∼2 dB sensitivity degradation from simulation to experiment is caused by the two PDs' response difference and other imbalances, which lead

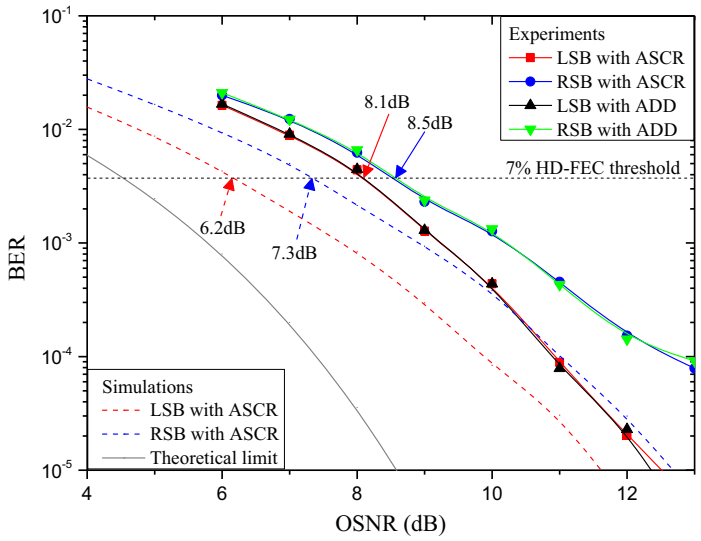

Fig. 7 Bit error rates versus OSNR from experiments and simulations of the ASCR and the ADD receiver. The theoretical limit is also plotted from: $\mathrm{BER} = \frac{1}{2}\,\mathrm{erfc}\left(\sqrt{B_{\mathrm{ref}}\frac{\mathrm{OSNR}}{R_S}}\right)$.[32,33]

to additional distortions of $I_1(n)$ and $I_2(n)$ in Eq. (4). Therefore, the performance of the ASCR is approximate to the ADD receiver when a strong LO is applied.

5 Optimal Design of OPBF and MIMO-AEQ for the ASCR

To reduce the influence of crosstalk, we can increase the width of the guard band or use OBPF with a high roll-off coefficient. However, increasing the width of the guard band decreases spectrum efficiency, and the OBPF with a high roll-off coefficient is of high expense. As the MIMO-AEQ algorithm deals with filtering damage and channel crosstalk simultaneously, the system can still achieve good performance without a high-expense OBPF or a larger guard band when MIMO-AEQ is strengthened. However, the performance of MIMO-AEQ is positively correlated with the number of taps of digital filters. In practical applications, the receiver cannot afford a large number of taps, which means great DSP computational resources and power requirements.

According to the above analysis of computational complexity and power consumption, the optical FRA of ASCR is suitable to realize high-speed signal processing for its low resource requirement. The simulations of the ASCR system are set with 50 Gbaud of 16 quadrature amplitude modulation (QAM) TSSB signal, the width of the guard band is 5 GHz, the roll-off coefficient of Nyquist shaping is 0.1, and the CSPR is 15 dB. The relationship between the number of digital filter taps required for MIMO-AEQ, the roll-off coefficient of OPBF, and the compensation effect can be analyzed synchronously.

Figure 8 shows the curve of the sensitivity of the LSB and RSB under different conditions. When CSPR = 15 dB, the sensitivities of LSB and RSB are rapidly improved with the increase of OBPF roll-off coefficient in the absence of MIMO-AEQ because a higher roll-off coefficient of OPBF helps the LSB and RSB suffer less filtering damage and crosstalk. When the roll-off coefficient reaches 600 dB/nm, the performance is no longer improved even with strengthened MIMO-AEQ because the high-performance OPBF is close to the ideal filter, eliminating the influence of the filtering damage and crosstalk. At this time, the corresponding sensitivity of the LSB and RSB channels is 18.8 and 19.6 dB, respectively, and the sensitivity gap of 0.8 dB is due to the greater effect of noise from Eqs. (4)–(6). The best LSB channel sensitivity is still 0.6 dB away to the theoretical limit[32,33] because there is still a small amount of SSBI/LRBI noise when CSPR = 15 dB.

Within MIMO-AEQ the sensitivity of LSB and RSB can be dramatically improved when low-expense OPBF is used (corresponding to the black lines and color lines in the region of low roll-off coefficient in Fig. 8). Take the LSB channel to achieve a receiving sensitivity of 19.1 dB as an example, the minimum roll-off coefficient of OPBF is 600 dB/nm without MIMO-AEQ. However, when the MIMO-AEQ with 15 taps is used, the same sensitivity can be achieved by

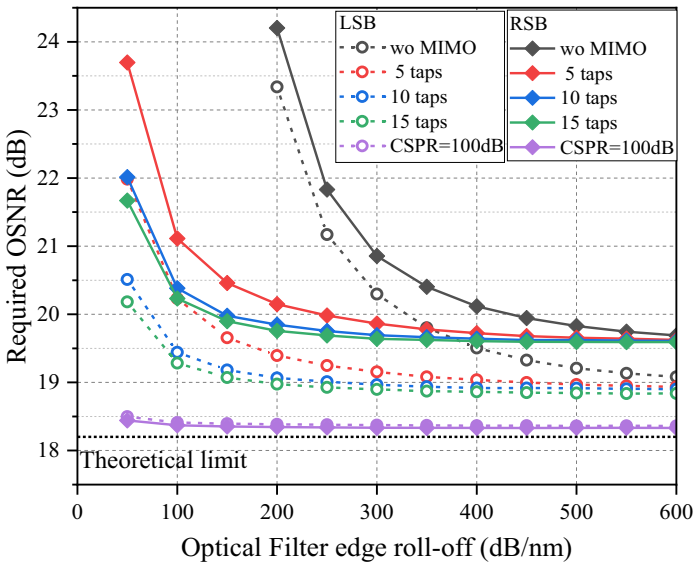

Fig. 8 Required OSNR versus roll-off coefficient and digital taps from LSB and RSB channels.

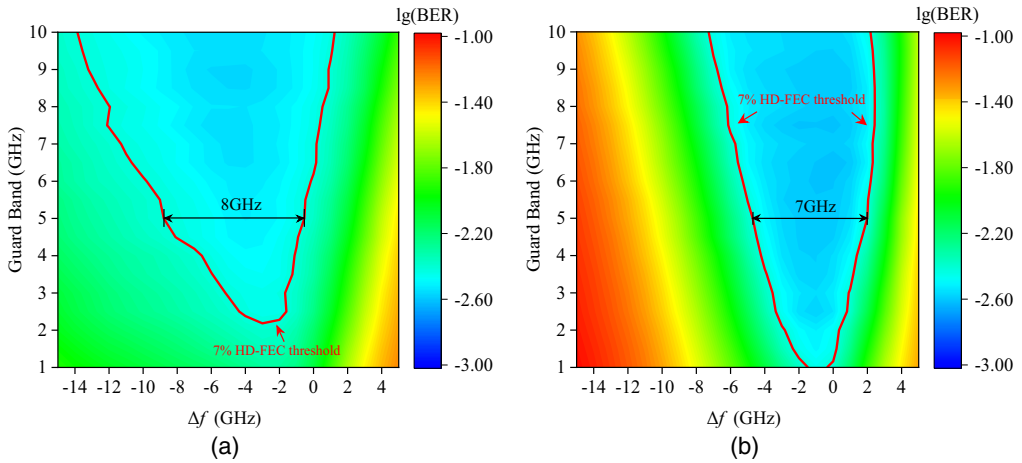

Fig. 9 BER degradation versus guard band and frequency offset under the (a) 100 dB/nm and (b) 500 dB/nm roll-off coefficient.

using a low-cost commercial OPBF with a roll-off coefficient of 150 dB/nm. Even if the taps are reduced to 10, the same sensitivity can be achieved by a 200 dB/nm OPBF. Therefore, the application of MIMO-AEQ greatly reduces the requirement of OPBF in the ASCR system.

Slightly increasing the number of digital filter taps of MIMO-AEQ can be achieved easily by utilizing more DSP computational resources. However, increasing the roll-off coefficient of OPBF means a complex manufacturing technology and a substantial increase in cost. Therefore, the design of the ASCR system should give priority to optimizing the performance of MIMO-AEQ. It can be seen from Fig. 8 that after the number of taps of the MIMO-AEQ filter reaches 10, the continuous increase in the number of taps no longer significantly improves the sensitivity performance. Therefore, to minimize the excessive waste of DSP computational resources, the number of taps of the digital filter is selected around 10. At this point, the ASCR system can achieve sufficient performance when the roll-off coefficient of OPBF reaches 200 dB/nm.

On the other hand, due to the manufacturing accuracy of commercial low-cost OBPF, there is usually a center wavelength (<0.01 nm) and 3 dB-band-pass width (~GHz) deviation. However, the ASCR system uses OBPF to accurately separate the LSB and RSB signals, so the bandwidth deviation and wavelength deviation of OBPF will affect the reception of TSSB signals. Toward 2 dB sensitivity degradation to the theoretical limit,[32,33] the OBPF deviation tolerance of the ASCR, which is shown in Fig. 9, is obtained by the RSB channel (relatively poor performance) under the typical roll-off coefficients of 100 and 500 dB/nm, respectively. Δf is the offset of the right edge of the trapezoidal OBPF relative to the signal center of TSSB. It can be seen that, while the width of the guard band is the same, although the OBPF with a low roll-off coefficient obtains poor optimal performance, its robustness is better as the blue area in the corresponding figure is larger. When the guard bandwidth is 5 GHz, the tolerance range of commercial low-cost OBPF for the ASCR is 8 GHz, which is better than that of 7 GHz when using high-performance OBPF. Above all, the ASCR can achieve a better balance in spectral efficiency, sensitivity performance, computational complexity, and system cost when the guard band is 5 GHz, the number of MIMO-AEQ taps is 10, and the roll-off coefficient of OPBF is around 200 dB/nm. With better robustness, the ASCR can still achieve good performance when using commercial optical filters at a low cost.

6 Conclusion

In summary, we design an ASCR based on a TSSB signal, and the FRA only requires one Hilbert operation, avoiding the nonlinear mathematical operation and the digital up-sampling. The power consumption of the proposed receiver can be reduced by 79.83% in the part of optical field reconstruction and dispersion compensation compared to the ADD receiver. Simulation and experiment results show that the average optical science noise ratio (OSNR) penalty of the proposed receiver is only 2 and 4 dB to the theoretical limit, respectively. With better robustness,

the ASCR also has a good balance between spectral efficiency, computational complexity, and optical filter cost. The optimal design indicates that the guard band is 5 GHz, the number of MIMO-AEQ taps is 10, and the roll-off coefficient of OPBF is around 200 dB/nm can help the proposed receiver achieve satisfactory sensitivity.

Code, Data, and Materials Availability

All data can be accessed by Ref. 34.

Acknowledgment

This work was supported by the Key Research and Development Program of Hubei Province (Grant No. 2022BAA054).

References

1. H. Kogelnik, "High-speed lightwave transmission in optical fibers," *Science*, **228**(4703), 1043–1048 (1985).
2. A. R. Chraplyvy et al., "8 × 10 Gb/s transmission through 280 km of dispersion-managed fiber," *IEEE Photonics Technol. Lett.* **5**(10), 1233–1235 (1993).
3. S. J. Savory, "Digital coherent optical receivers: algorithms and subsystems," *IEEE J. Sel. Top. Quantum Electron.* **16**(5), 1164–1179 (2010).
4. S. Bigo, "Coherent optical long-haul system design," in *Proc. Opt. Fiber Comm. Conf.*, p. OTh3A.1 (2012).
5. I. P. Kaminow, T. Li, and A. E. Willner, *Optical Fiber Telecommunications V Volume B Systems and Networks*, Chap. 2, Elsevier Science Limited (2008).
6. X. Zhou, "Efficient clock and carrier recovery algorithms for single-carrier coherent optical systems: a systematic review on challenges and recent progress," *IEEE Signal Process. Mag.* **31**(2), 35–45 (2014).
7. L. G. Kazovsky, G. Kalogerakis, and W. Shaw, "Homodyne phase-shift-keying systems: past challenges and future opportunities," *J. Lightwave Technol.* **24**(12), 4876–4884 (2016).
8. L. Gagnon et al., "Coherent detection of optical quadrature phaseshift keying signals with carrier phase estimation," *J. Lightwave Technol.* **24**(1), 12–21 (2006).
9. S. T. Le, V. Aref, and J. Cho, "Single-ended coherent receiver," *J. Lightwave Technol.* **40**(5), 1382–1399 (2021).
10. A. Mecozzi, C. Antonelli, and M. Shtaif, "Kramers–Kronig coherent receiver," *Optica* **3**(11), 1220–1227 (2016).
11. K. Zou et al., "Spectrally efficient terabit optical transmission with Nyquist 64-QAM half-cycle subcarrier modulation and direct-detection," *Opt. Lett.* **41**(12), 2767–2770 (2016).
12. Z. Li et al., "Two-stage linearization filter for direct-detection subcarrier modulation," *IEEE Photonics Technol. Lett.* **28**(24), 2838–2841 (2016).
13. M. S. Erkilinc et al., "Reach enhancement for WDM direct-detection subcarrier modulation using low-complexity two-stage signal-signal beat interference cancellation," in *Proc. Eur. Conf. Opt. Commun.*, p. M.2.B.1 (2016).
14. Z. Li et al., "SSBI Mitigation and the Kramers–Kronig scheme in single-sideband direct-detection transmission with receiver-based electronic dispersion compensation," *J. Lightwave Technol.* **35**(10), 1887–1893 (2017).
15. T. Bo and H. Kim, "Kramers–Kronig receiver operable without digital upsampling," *Opt. Express* **26**(11), 13810–13818 (2018).
16. Z. Li et al., "Joint optimization of resampling rate and carrier-to-signal power ratio in direct-detection Kramers–Kronig receivers," in *Proc. Eur. Conf. Opt. Commun.*, p. W.2.D.3 (2017).
17. B. Corcoran, B. Foo, and A. J. Lowery, "Single-photodiode per polarization receiver with signal-signal beat interference suppression through heterodyne detection," *Opt. Express* **26**(3), 3075–3086 (2018).
18. S. Fan et al., "Twin-SSB direct detection transmission over 80km SSMF using Kramers–Kronig receiver," in *Proc. Eur. Conf. Opt. Commun.*, pp. 1–3 (2017).
19. S. Fan et al., "Comparison of Kramer–Kronig receiver and one-stage SSBI mitigation algorithm in twin-SSB direct detection transmission systems enabled by MIMO processing," *Opt. Commun.* **434**, 75–79 (2019).
20. X. Li et al., "Asymmetric direct detection of twin-SSB signals," *Opt. Lett.* **45**(4), 844–847 (2020).
21. X. Li et al., "Asymmetric self-coherent detection," *Opt. Express* **29**(16), 25412–25427 (2021).
22. X. Li et al., "Asymmetric self-coherent detection based on mach-zehnder interferometers," *J. Lightwave Technol.* **40**(7), 2023–2032 (2022).
23. C. Yu et al., "Experimental demonstration of twin-single-sideband signal detection system based on a single photodetector and without optical bandpass filter," *Opt. Express* **30**(21), 37341–37349 (2022).

24. K. Zhou et al., "Design of the real-time single-photodiode digital coherent receiver suitable for free space optical communication," *IEEE Photonics J.* **12**(5), 1–12 (2020).
25. K. Zhou et al., "A method to reduce the algorithm complexity of the single-photodiode-per-polarization coherent receiver," *IEEE Photonics J.* **12**(1), 1–12 (2020).
26. P. Duhamel and M. Vetterli, "Fast fourier transforms: a tutorial review and a state of the art," *Signal Process.* **19**(4), 259–299 (1990).
27. L. Marple, "Computing the discrete-time "analytic" signal via FFT," *IEEE Trans. Signal Process.* **47**(9), 2600–2603 (2002).
28. C. Füllner et al., "Transmission of 80-GBd 16-QAM over 300 km and Kramers–Kronig reception using a low-complexity FIR Hilbert filter approximation," in *Proc. Opt. Fiber Commun. Conf.*, p. W.4.E.3 (2018).
29. T. Bo and H. Kim, "Toward practical Kramers–Kronig receiver: resampling, performance, and implementation," *J. Lightwave Technol.* **37**(2), 461–469 (2019).
30. N. Diamantopoulos, B. Shariati, and I. Tomkos, "On the power consumption of MIMO processing and its impact on the performance of SDM networks," in *Proc. Opt. Fiber Commun. Conf.*, p. Th2A.18 (2017).
31. D. Kilper et al., "Power trends in communication networks," *IEEE J. Sel. Top. Quantum Electron.* **17**(2), 275–284 (2011).
32. J. G. Proakis and S. Masoud, *Digital Communications*, Chap. 4, McGraw-Hill, New York (2001).
33. I. Kaminow, T. Li, and A. E. Willner, *Optical Fiber Telecommunications VB: Systems and Networks*, Chap. 2, Elsevier (2010).
34. K. Zhou, "Figures of Asymmetric simplified coherent receiver based on twin-SSB signal realizes ultra-low computational complexity," *Figshare*, 2023, https://doi.org/10.6084/m9.figshare.23734422.

Keji Zhou received his PhD from Huazhong University of Science and Technology. He is currently in a joint postdoctoral workstation and studying novel optical field reconstruction techniques and digital distortion compensation algorithms.

Tianming Li received his MS degree from Huazhong University of Science and Technology, Wuhan, China. He has worked at Fiberhome Telecommunication Technologies Co., Ltd., since 2022. His research interests include coherent digital signal processing and forward error correction techniques.

Yaqin Wang was a senior engineer responsible for R&D work in Fiberhome Telecommunication Technologies Co., Ltd., and engaged in optical transport network techniques for 20 years. She has a wealth of project research and development experience and accumulated many invention patents.

Sheng Cui received his PhD in radio physics from Xidian University, Xi'an, China. He has been an associate professor at the School of Optical and Electronic Information, Huazhong University of Science and Technology, since 2011. His research interests include novel coherent detection, intelligent optical performance monitoring, distortion compensation techniques for free space, and fiber optical communication systems. He is a member of IEEE.

Ming Wei was a senior engineer responsible for R&D work in Wuhan Fiberhome Technical Services Co., Ltd. and engaged in communication research and development work for 18 years. He has a wealth of project research and development experience and accumulated many invention patents.

Yong Xiao is an associate group leader of IMT-2030 (6G) Network Intelligence Group and vice director of 5G Verticals Innovation Laboratory. He has been a professor at the School of Electronic Information and Communications, Huazhong University of Science and Technology, since 2018. His research interests include next-generation wireless technology and semantic communications.